



Influence of Stroke on Performance Characteristics of Synthetic Jet Fan

K. Nishibe^{1†}, Y. Nomura², K. Noda², H. Ohue¹, and K. Sato³

¹ Department of Mechanical Engineering, Tokyo City University, Setagaya, Tokyo 158-8557, Japan

² Graduate School of Engineering, Tokyo City University, Setagaya, Tokyo 158-8557, Japan

³ Department of Mechanical System Engineering, Kogakuin University, Shinjuku, Tokyo 160-0016, Japan

†Corresponding Author Email: knishibe@tcu.ac.jp

(Received October 6, 2017; accepted March 18, 2018)

ABSTRACT

Synthetic jets, whose size and weight can be reduced easily, have become an attractive alternative to continuous jets. Many experimental and numerical studies have been conducted on synthetic jets to investigate their fundamental flow characteristics, including jet structure, for applied research such as boundary layer control and enhanced fluid mixing. However, few studies have focused on fluid transportation devices using synthetic jets as a driving source. Therefore, several issues concerning fluid transport characteristics still need to be resolved. In addition, although optimum operation of devices using synthetic jets is essential for their practical use, few studies have focused on this issue. The present study experimentally demonstrates the influence of the dimensionless stroke L on the performance characteristics of a synthetic jet fan under Reynolds number $Re = 1800$ and the same fan geometry; here, the stroke l is nondimensionalized by the primary slot width b . Furthermore, numerical simulations are conducted to complement the experiment. Velocity and pressure measurements are performed using a hot-wire anemometer, differential pressure manometer, and pressure transducer. The influence of the dimensionless stroke L on the performance/efficiency curves, static pressure distribution on the duct surface, and unsteady flow characteristics are investigated. Moreover, the flow field inside the duct is observed through numerical simulation. The results show that the performance characteristics and pressure recovery process depend on the dimensionless stroke L , and an optimum range of dimensionless stroke L exists for operation.

Keywords: Synthetic jets; Jet pump; Fan performance curve; Pressure recovery.

NOMENCLATURE

b	slot width ($= 5.0 \times 10^{-3}$ m)	t	time
d	duct length ($= 0.6$ m)	T	period
f	frequency	u	velocity in the x -direction
h	slot and duct span length ($= 2.0 \times 10^{-2}$ m)	$ u $	absolute velocity in the x -direction
l	stroke length	U	representative velocity
L	dimensionless stroke length for the synthetic jet ($= l/b$)		$(= fl = \frac{1}{T} \int_0^{T/2} U_{sa} \sin 2\pi f t dt)$
p	static pressure	U_{sa}	velocity amplitude in a synthetic jet at the slot exit
Δp	pressure difference between the inlet and outlet of the device	w	duct width ($= 5.0 \times 10^{-2}$ m)
p^*	dimensionless static pressure ($= p/0.5\rho U^2$)	x, y, z	coordinate axes
Q_d	flow rate at mixing duct outlet	η	efficiency ($= \Delta p Q_e / 0.5\rho U^2$)
Q_e	entrainment flow rate	ν	kinematic viscosity
Q_p	flow rate from a primary slot ($= bhU$)	ρ	density
Re	Reynolds number ($= Ub/\nu$)	Φ	flow rate coefficient for the synthetic jet ($= Q_e / bhU$)
s	spacing of the primary nozzle from mixing duct inlet	Ψ	pressure coefficient for the synthetic jet ($= \Delta p / 0.5\rho U^2$)
		ω	vorticity in z -direction

1. INTRODUCTION

Jet pumps that use a jet flow as a motive fluid have long

been applied in various fields, and fundamental studies have investigated the pressurizing mechanism and behavior of the internal flow field and optimum

operating and geometry conditions to improve their performance and efficiency (Hoshi *et al.* 1964; Sanger 1970; Narui and Inagaki 1991; Huang *et al.* 1999; Narabayashi *et al.* 2006; Yamazaki *et al.* 2007; Little *et al.* 2015; Xiao *et al.* 2016). Motive fluid ejected from the nozzle of the jet pump involves fluid from the surroundings, and discharges to a throat/duct. Jet pumps have a simple structure, with no internal rotating parts. Therefore, they have been applied as cooling water circulation pumps for safety in atomic reactors and as ejectors for enhancing the mixing and adjusting petroleum components in energy plants that require continuous, safe operation. However, these systems are large and complicated because they require large rotating machines such as centrifugal compressors to generate a continuous flow of motive fluid. Thus, the applications of jet pumps remain limited.

Considering these shortcomings, there is an urgent need to greatly reduce the size and weight of the whole system. Of late, as an alternative to continuous jets, studies have focused on synthetic jets, because these use actuators such as a piezoelectric devices and compact speakers, whose size and weight can be reduced easily. Free synthetic jets formed by iterative ejection and suction at the slot/nozzle exit have been widely studied. Their fundamental flow characteristics such as the criteria for generating/developing formed jets and influence of stroke on jet flow structure (Holman *et al.* 2005; Shuster *et al.* 2007; Nishibe *et al.* 2011; Koso and Morita 2014) have been clarified for applications such as active control for flow separation and aerodynamic drag over an airfoil (Amity *et al.* 2001; Whitehead *et al.* 2006; Cattafesta *et al.* 2011; Yen and Ahmed 2012). One application is fluid machinery using synthetic jets as their driving source (Abdou 2014; Park *et al.* 2002; Ohuchi *et al.* 2005; Xia and Zhong 2012, 2013; Koso and Nakashima 2008). For example, Abdou (2014) discussed the characteristics of a T-type micropump using synthetic jets by investigating the time variation of the flowrate and its maximum pressure through both experiments and numerical simulations. Luo *et al.* (2005) proposed a novel synthetic jet pump with a dividing-clapboard installed downstream of the slot instead of a duct to resolve issues such as fluid leakage and duct clogging faced in conventional jet pumps. Mahalingam *et al.* (2004) demonstrated the effectiveness of temperature control in a two-dimensional channel flow by using a synthetic jet ejector. Koso and Nakajima (2008) discussed the influence of a nozzle geometry and vibration characteristics of an actuator on the performance characteristics of a fan using synthetic jets generated by a piezoelectric device. Ishizawa *et al.* (2015) proposed a novel synthetic jet fan that actively used not only an ejection cycle but also a suction cycle of the synthetic jet to generate more momentum, and they discussed its performance through an experiment.

However, many issues still remain to be addressed before synthetic jets can be used practically as the driving source of fluid machines. For example, it is essential to establish optimum operating conditions for such machines through detailed studies. Holman

and Utturkar (2005) and Koso and Morita (2014) clarified the criteria for generating/developing free synthetic jets and the influence of the dimensionless stroke on the unsteady flow characteristics of these jets. However, few studies have investigated the influence of the dimensionless stroke on the pump/fan performance and efficiency. Furthermore, medical machines need highly precise flowrate measurements, and repetitive stresses in machines could cause serious accidents in energy plants; therefore, velocity and pressure fluctuations need to be suppressed to the maximum extent possible. More importantly, the frequencies of such fluctuations should be kept from approaching the natural vibration frequencies of machines. At the same time, there are cases in which the application of fluctuations under appropriate oscillating conditions is more effective for transporting fluids with mixing and cooling. Thus, to use oscillating synthetic jet fans/pumps as a driving source, it is essential to determine their performance characteristics, including the oscillating characteristics of the internal flow field.

2. EXPERIMENTAL AND NUMERICAL SETUP

Figure 1 shows the experimental apparatus for a synthetic jet fan. Figure 1(a) shows a schematic drawing of the synthetic jet fan system; this system consists of a speaker-type actuator, a motive (primary) slot, a suction/mixing duct, a plenum tank, and a booster fan. Figures 1(b) and 1(c) show details of the primary slot and mixing duct, respectively. Air was used as the working fluid, and the secondary jet was sucked from the atmosphere via the entrainment induced by the motive synthetic jet blowing from the primary slot; both jets were mixed and pumped to the duct. Then, the kinetic energy of the mixed flow was recovered to the static pressure passing through the duct and discharged to the plenum tank. The synthetic jet was generated by driving the speaker (Diecook D-15L). The representative velocity for synthetic jet U was obtained by calculating the time-averaged centerline velocity of the blowing cycle at the contraction part inside the primary slot ($x/b = -6$) over the blowing and suction cycles. Here, the time-averaged centerline velocity at $x/b = -6$ was regarded as the time- and spatial-averaged velocity because the velocity profile at $x/b = -6$ is almost uniformly distributed along the slot width and span direction. The definition of the representative velocity is shown below (Holman and Utturkar 2005):

$$U = \frac{1}{T} \int_0^{T/2} U_{sa} \sin 2\pi f t dt \quad (1)$$

where f and T are the velocity fluctuation frequency and period, respectively, and U_{sa} is the velocity amplitude at the center of the slot. Another important parameter is the dimensionless stroke L , where the stroke l is nondimensionalized by the primary slot width b (Holman and Utturkar 2005). In this study, controlling the velocity fluctuation frequency f of the synthetic jets at the slot exit under the same amplitude U_{sa} . The absolute velocities along the duct

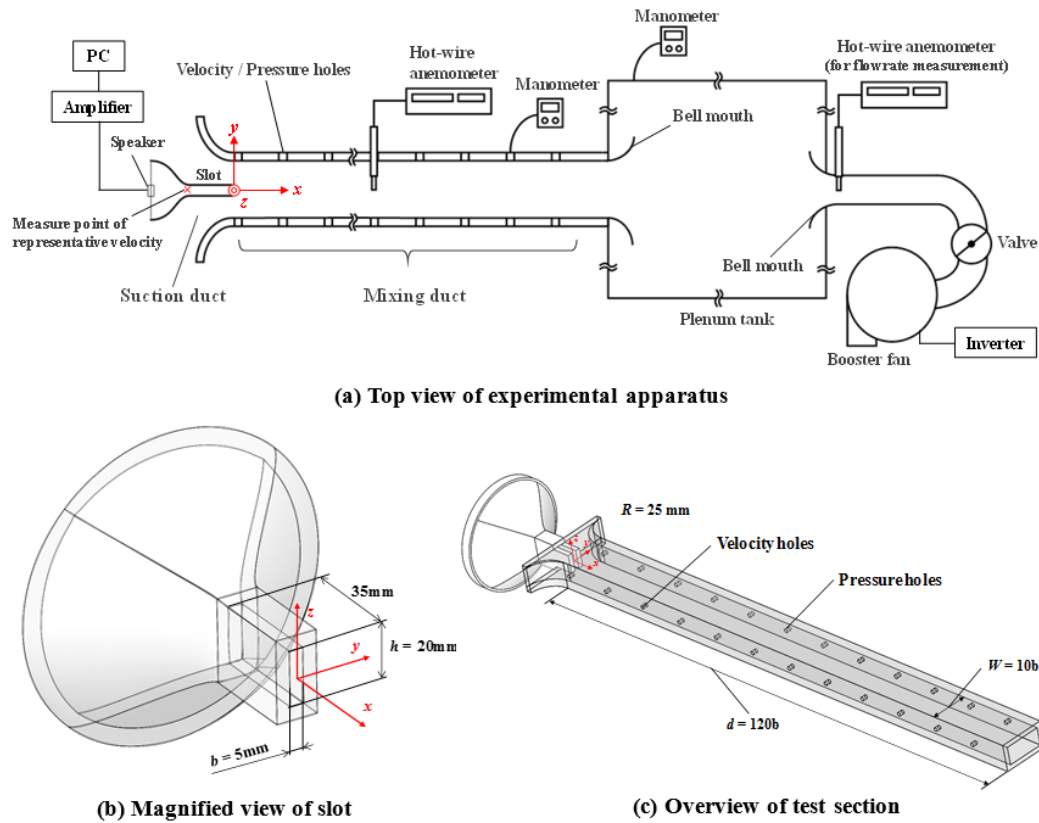


Fig. 1. Experimental apparatus.

the dimensionless stroke L was adjusted by center $|u|$ were measured by using single I-type hot-wire anemometer (Kanomax 7000 series). The velocities obtained using the hot-wire anemometer were considered the absolute velocities in the x -direction $|u|$ because the x -velocity component along the duct center is markedly greater than that in the y - and z -directions. The entrainment flow (secondary flow) rate Q_e is estimated based on the flow rate at the mixing duct outlet Q_d . Q_d is calculated from the area of the circular pipe and the time-averaged velocity distribution at the circular pipe immediately downstream of the bell-mouth using the I-type hot-wire anemometer. Note that the time-averaged flow rate at the slot exit over the cycle is zero for synthetic jets. Therefore, the flow rate at the mixing duct is equal to the entrainment flow rate ($Q_e = Q_d$). From the preliminary experiment, it was confirmed that the velocity distribution at the flow rate measurement area was approximately equal to that in the measurement range of the flow rate in this study. The time-averaged pressure distribution and pressure fluctuation on the duct surface were measured using a differential pressure manometer (Okanoworks, DMP301N) and a pressure transducer (JTEKT, PD104K) with amplifiers, and these data were analyzed using a Fast Fourier transform analyzer. The discharge pressure ΔP is time-averaged from the measured differential pressure between the static pressure at the plenum tank and the inlet of the secondary flow (atmospheric pressure) by using the differential pressure manometer. To investigate the performance characteristics, the performance and efficiency curves are described by the flow rate

coefficient, pressure coefficient, and efficiency of the synthetic jets as follows:

$$\Phi = \frac{Q_e}{bhU} \quad (2)$$

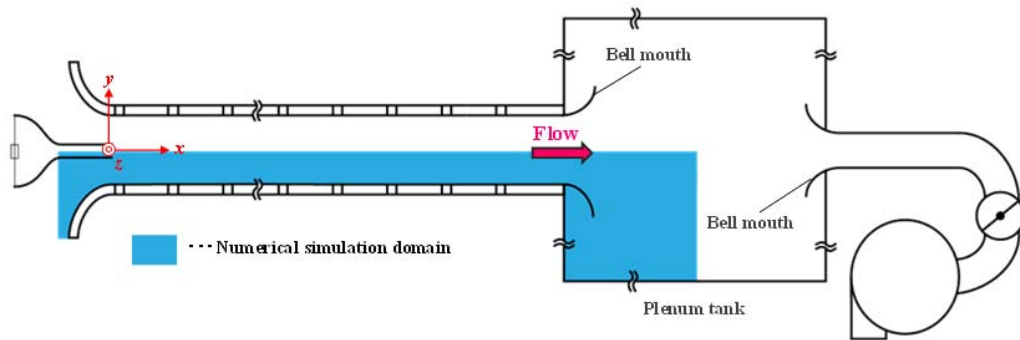
$$\Psi = \frac{\Delta P}{0.5\rho U^2} \quad (3)$$

$$\eta = \Phi\Psi \quad (4)$$

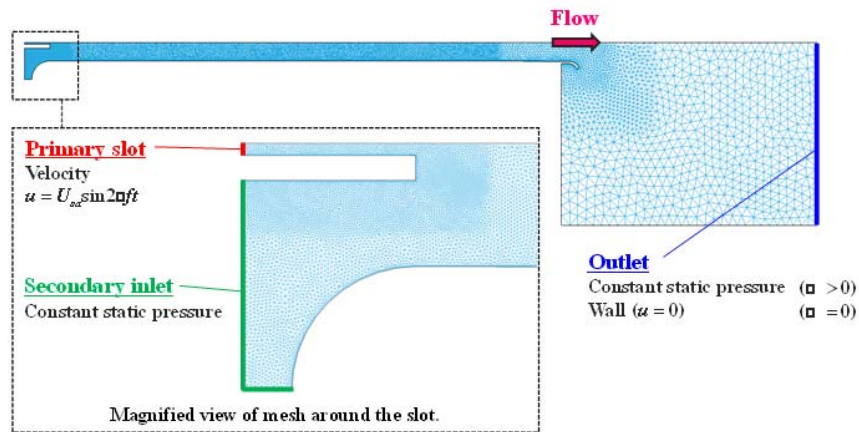
where ρ is the density of air. In the present study, experiments and numerical simulations were conducted for $10 \leq L \leq 160$ under the same Reynolds number $Re = 1800$ and the same fan geometry, such as a rectangle-shaped motive slot with width $b = 5.0 \times 10^{-3}$ m and span length $h = 2.0 \times 10^{-2}$ m and rectangular mixing duct with length, width, and span length of $d = 0.6$ m, $w = 5.0 \times 10^{-2}$ m, and $h = 2.0 \times 10^{-2}$ m, respectively, as shown in Figs. 1(b) and 1(c). Note that the Reynolds number was defined based on the slot width b as the representative length and the kinetic viscosity of air ν , and the representative velocity U . The Reynolds number of 1800 was selected as appropriate for conducting the experiment because it is the stable operational condition of the speaker-type synthetic jet generator for various L values in the present study.

Figure 2 shows the numerical domain and boundary conditions. Panels (a)-(c) indicate the correspondence of domains between the experiment and numerical simulation, boundary condition and mesh of the x - y plane with a magnified view of the

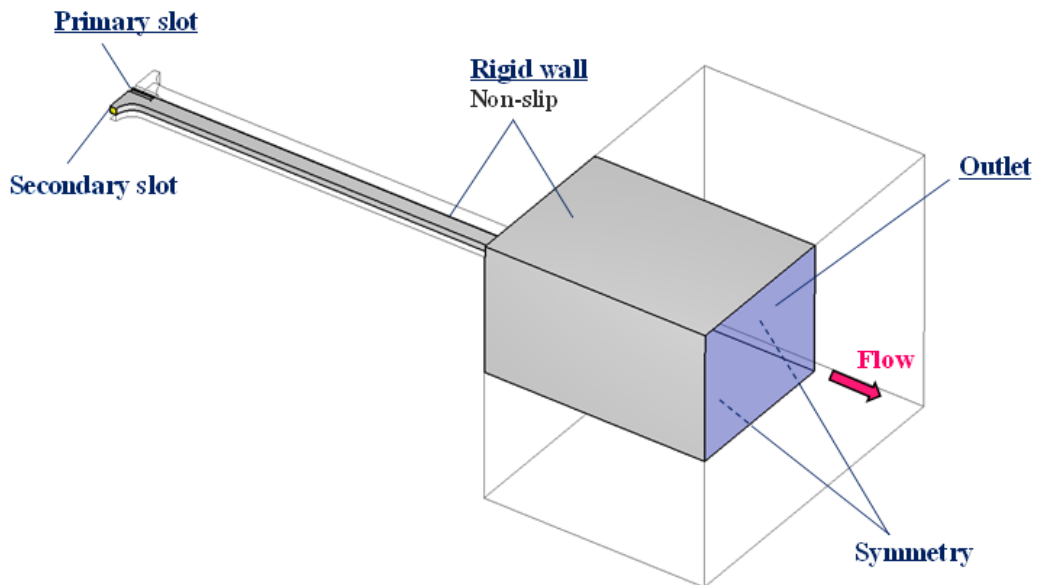
primary/secondary slot, and bird's eye view of the



(a) Correspondence of domains between the experiment and numerical simulation



(b) Boundary condition and mesh of x - y plane with magnified view of the primary/secondary slot



(c) Bird's eye view of the overall numerical model

Fig. 2. Numerical domain and boundary conditions.

overall numerical model, respectively. The SC/Tetra commercial computer fluid dynamics code (Software Cradle Co., Ltd.) was used in the

numerical simulation. In accordance with previous numerical works that assumed an incompressible viscous flow and that applied the Reynolds averaged

Navier-Stokes (RANS) simulation for free synthetic jet flow fields (Tang and Zhong 2005; Zhang *et al.*

2007; Kobayashi *et al.* 2017), in this study, the numerical simulation was performed assuming a 3D

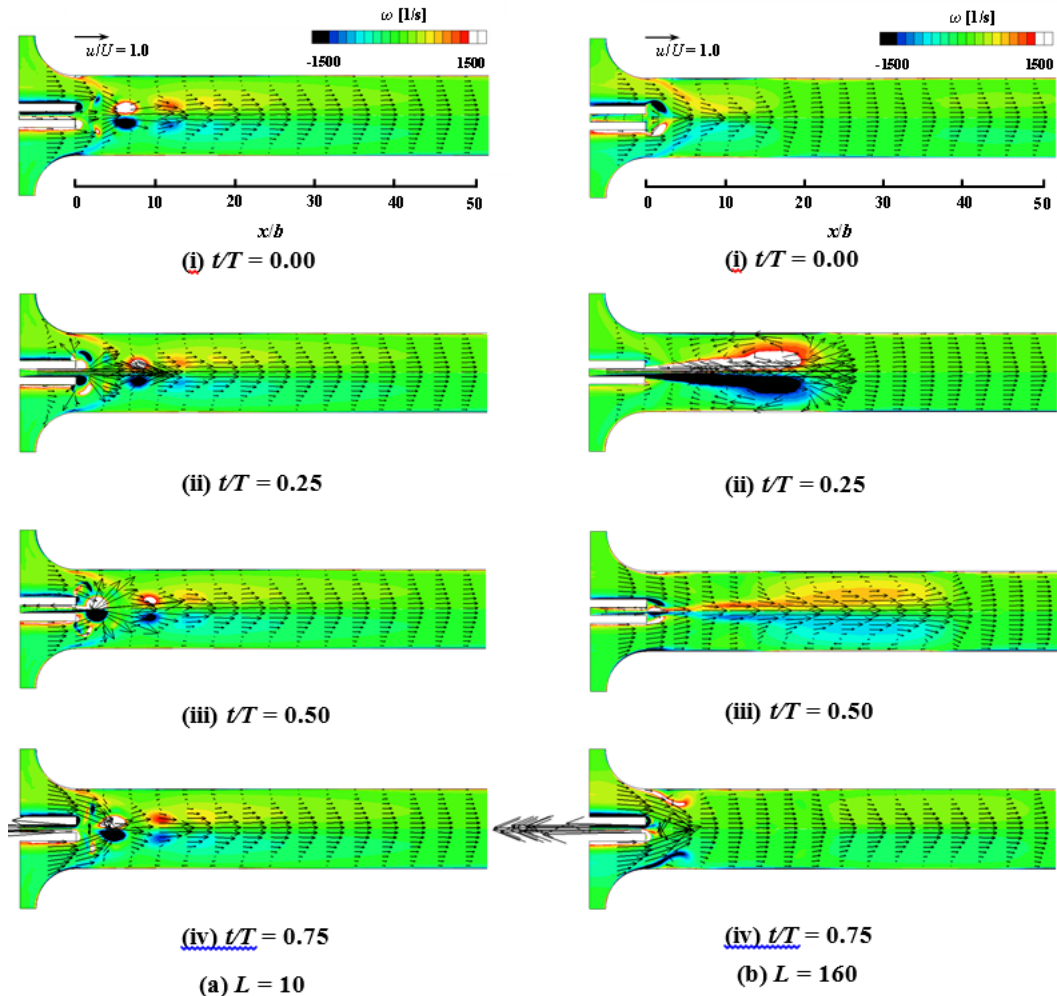


Fig. 3. Time variation of the velocity vectors and vorticity distribution at mid-span from the numerical simulation ($z/h = 0$, $\Phi \approx 2.5$).

incompressible viscous flow and by using the RANS simulation with the standard $k-\epsilon$ turbulent model. In addition, based on preliminary examination for free synthetic jet model to select/use turbulence models, numerical results with the standard $k-\epsilon$ turbulent model were found to match with those of the experiment (e.g. time variation of the position of the vortex pair) more than others (e.g., Laminar flow, $k-\omega$). The numerical model shows geometric symmetry around the $x-y$ and $x-z$ planes with approximately 2,360,000 mesh points, assuming the fan internal flow is symmetric to these planes (quarter model highlighted in Fig. 2). The dependence of the mesh resolution was confirmed in this study. Over 1,580,000 mesh points were comparable to those of experimental data. Therefore, we selected the model with approximately 2,360,000 mesh points. For simplification, a sine wave $u = U_{sa} \sin 2\pi ft$ is applied to the fluid velocity at the primary slot instead of a moving boundary condition (Tang and Zhong 2005). The constant static pressure condition is applied to the mixing duct inlet and outlet of the plenum tank ($\Phi > 0$), and the nonslip condition is applied to the rigid walls including the outlet of the plenum tank for

zero flowrate ($\Phi = 0$) in the test facility.

Figure 3 shows the time variation of the velocity vectors and vorticity distribution at mid-span over one cycle from the numerical simulation ($z/h = 0$, $\Phi \approx 2.5$, $Re \approx 1800$). Panels (a) and (b) indicate the results for $L = 9$ and 146, respectively. Panels (i)-(iv) indicate the results at dimensionless time $t/T = 0.0$ (stopping of suction/starting of blowing), 0.25 (maximum blowing), 0.5 (stopping of blowing/starting of suction) and 0.75 (maximum suction), respectively. In this figure, during the blowing process (panels (ii) and (iii)), a vortex pair generated near the slot exit translates downstream of the mixing duct, and inflow simultaneously occurs from the suction duct induced by an entrainment—induced by the formation and development of the vortex pair. In addition, the vortex pair translates while maintaining its vortex structure further downstream for $L = 146$ than that for $L = 9$. This vortex behavior is similar to that for free synthetic jets. The flow field during the suction phase differs between the free synthetic jet and the present synthetic jet fan. In the free synthetic jets. Suction

flow occurs from downstream of the slot to the slot exit (back flow) during suction from the entire field; whereas, in the case of the present synthetic jet fan,

for which the conditions involve a lack of exposure to the external environment, and the presence of a pressure gradient, slight back flow during suction

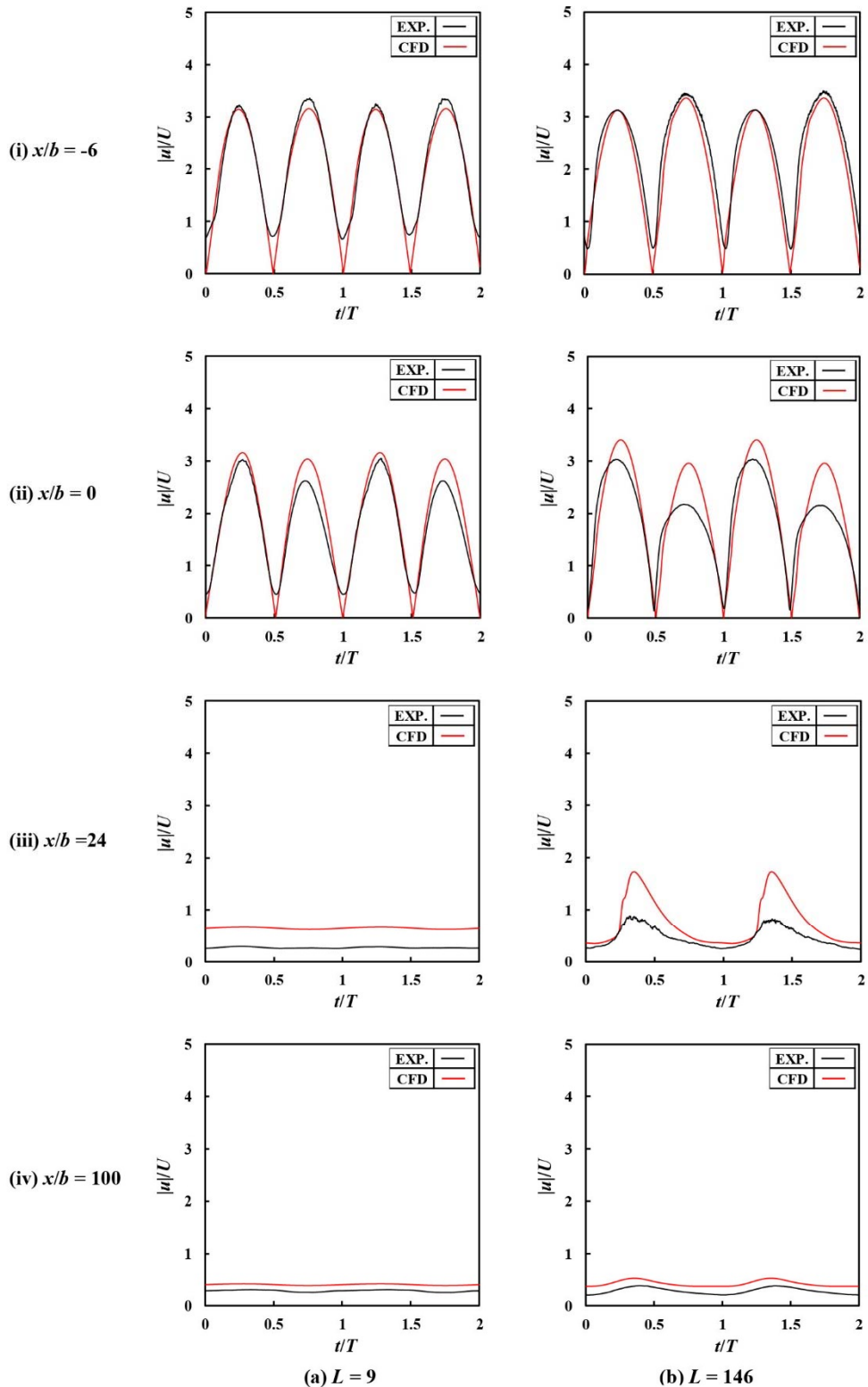


Fig. 4. Velocity waveform along jet centerline ($\Phi \approx 2.5$, $y/b = 0$, $z/b = 0$).

from the downstream of the mixing duct is noted because the flow is mainly drawn from the suction duct towards the synthetic jet fan. In addition, a part of

the induced flow from the suction duct was found to flow to the mixing duct without suctioning to the slot interior. Furthermore, from the velocity vectors, the

velocity distribution in the form of jet flow was generated in the mixing duct. Further downstream, the velocity distribution changed to a duct-like flow. Thus, if unsteady characteristics are disregarded, the jet

structure is assumed to form with a momentum in the mixing duct and a decrease in the momentum downstream induces a pressure increase similar to that of the conventional jet fan using the continuous jet.

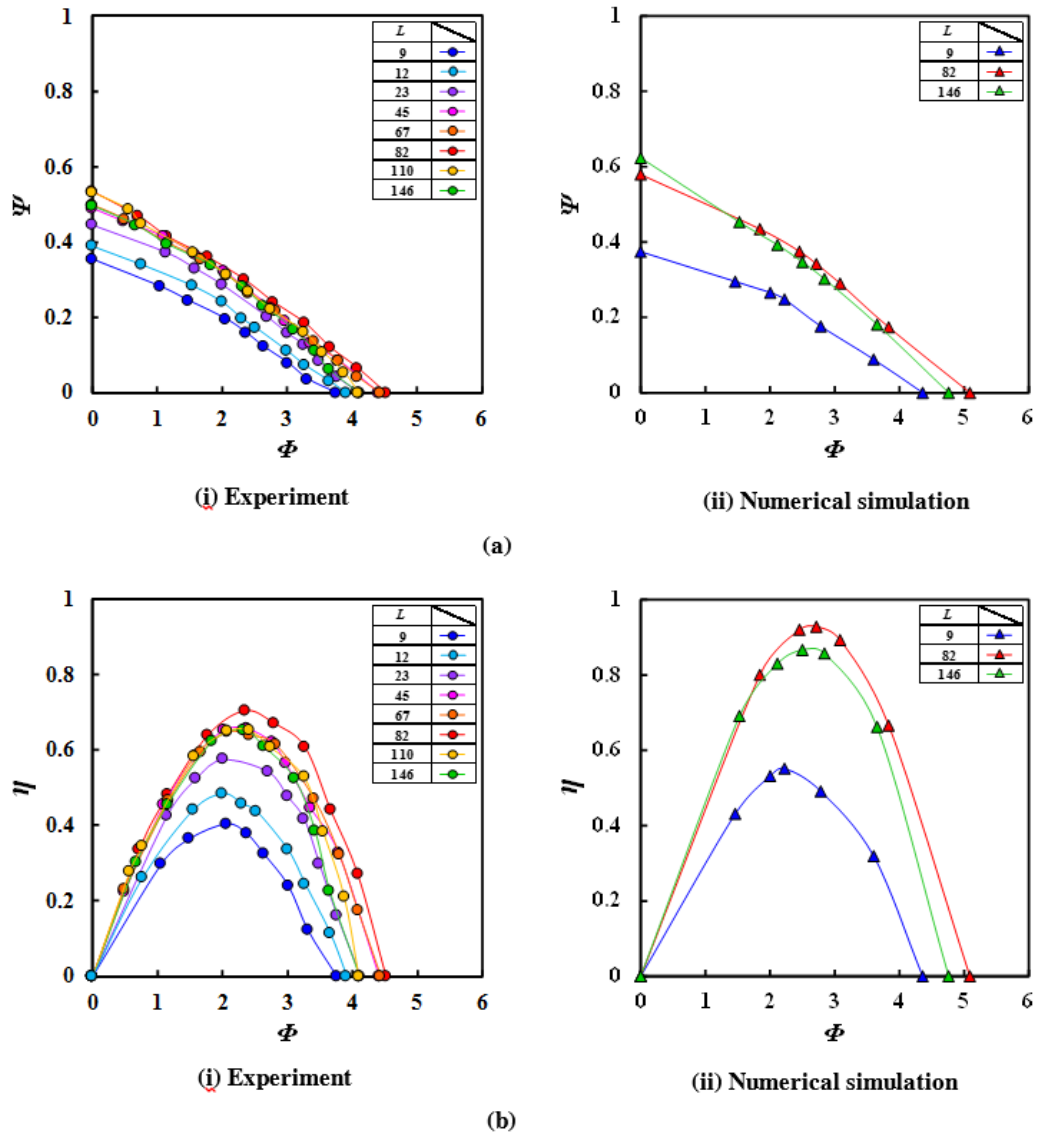


Fig. 5. Influence of dimensionless stroke on performance and efficiency curves.

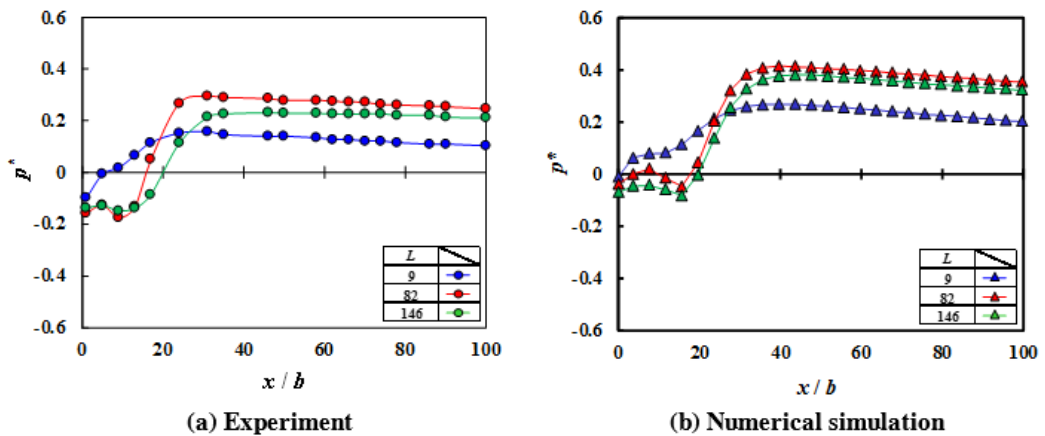


Fig. 6. Mixing duct wall pressure distribution ($\Phi \approx 2.5$).

Figures 4(a) and 4(b) show the time variation of the dimensionless absolute velocity along the jet centerline ($y/b = z/b = 0$) for synthetic jets $L = 9$ and 146, respectively, for $\Phi \approx 2.5$. The results obtained using the hot-wire anemometer and the numerical simulations are indicated by the black and red lines,

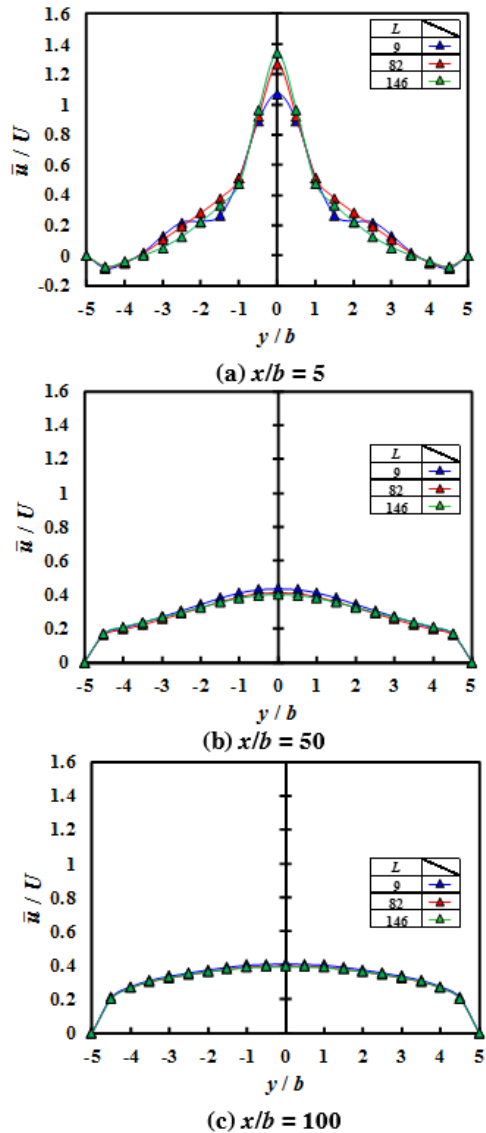


Fig. 7. Typical instantaneous velocity distribution on mid-span from numerical simulation ($\Phi \approx 2.5$, $z/h = 0$).

respectively. Panels (i)–(iv) show the results for $x/b = -6, 0, 24$, and 100, respectively. The horizontal axis represents the dimensionless time t/T , where T is the jet blowing and suction cycle period for each stroke, and the vertical axis represents the dimensionless absolute velocity $|u|/U$. The experimental results for the velocity profile and its decay process along the jet centerline are qualitatively similar to the numerical ones. The velocity waveforms at the slot exit for $x/b = 0$ are shown in Panels 4(a)(ii) and 4(b)(ii), and the first and second peaks corresponding to the blowing and suction phases and the fluctuating frequency are double the actuator frequency. For $L = 9$, the first

peak formed by blowing attenuates with increasing x/b , and the resulting waveform at $x/b = 24$ shows much smaller velocity fluctuation than that for $L = 146$, as in a typical pulsating jet. In addition, the velocity fluctuation for $L = 146$ and $x/b = 100$ at the duct exit is also higher than that for $L = 9$ and $x/b = 24$. Therefore, it is considered that the amplitude of the outlet flow through the duct increases with L . Section 3.2 provides some details of the influence of L on the velocity fluctuation.

3. RESULTS AND DISCUSSION

3.1 Performance characteristics

Figure 5 shows the influence of L on the pressure performance and efficiency as determined through an experiment and a numerical simulation. Panels (a) and (b) show the dimensionless pressure performance curves (Φ - Ψ) and dimensionless efficiency curves (Φ - η), respectively. Note that the representative velocity U was defined as expressed in formula (1) according to Holman and Utturkar (2005), in which the flowrate generated during the blowing process over the cycle is considered because the synthetic jet is unsteady flow with net-zero-flowrate. Thus, squaring the time-averaged velocity at the slot has no physical significance. Therefore, the representative velocity is an expediential value; the meanings of Φ and Ψ are relative and simply used to compare the results among various L values in Fig. 5(a). For simplicity, the efficiency η in Fig. 5(b) is defined as $\eta = \Phi\Psi$ in this study. Generally, η should be indicated as hydraulic power/input power or hydraulic power/shaft power. However, in case of the synthetic jets, electricity is consumed or power is used during not only blowing but also suction. Therefore, future research will focus on discussing in detail the optimum evaluation for the performance/efficiency of the synthetic jet fans. The experimental and numerical simulation results in panels (i) and (ii), respectively, showed good qualitative agreement considering that the performance curves for $L = 82$ and 146 are comparable, and they are higher than those for $L = 9$. The dimensionless pressure performance curves in Fig. 5(a) had negative slopes regardless of L . These results generally agreed with those obtained in previous studies for asymmetrical synthetic jet fan under low dimensionless stroke range $L < 5$ (Koso and Nakajima 2008) and a conventional jet pump/fan using a continuous jet (Ishizawa *et al.* 2015). On the other hand, the experimental results in Fig. 5(a)(i) indicate that the maximum pressure coefficient Ψ_{max} and maximum flowrate coefficient Φ_{max} clearly increases with L for $9 \leq L \leq 45$ but show no obvious differences for $L = 45 \leq L \leq 146$ in this study. As a result, the dimensionless efficiency curves obtained by the product of Φ and Ψ , as shown in Fig. 5(b)(i), were concave down and formed a larger arc with increasing L for $9 \leq L \leq 45$, and curves for $67 \leq L \leq 146$ were roughly distributed as one curve in Fig. 5(b)(i). Note that the dimensionless flowrate Φ , pressure coefficient Ψ , and efficiency η are defined based on the representative velocity U that considers

only the blowing cycle of the motive synthetic jet. In addition, the efficiency was not calculated based on input power into the actuator. Thus, these values are relatively higher than those for typical fluid machines, including conventional continuous jet

pumps, and there is a condition under which η_{max} approximately reaches unity.

Figures 6(a) and (b) show the time-averaged mixing duct wall pressure distribution obtained from the

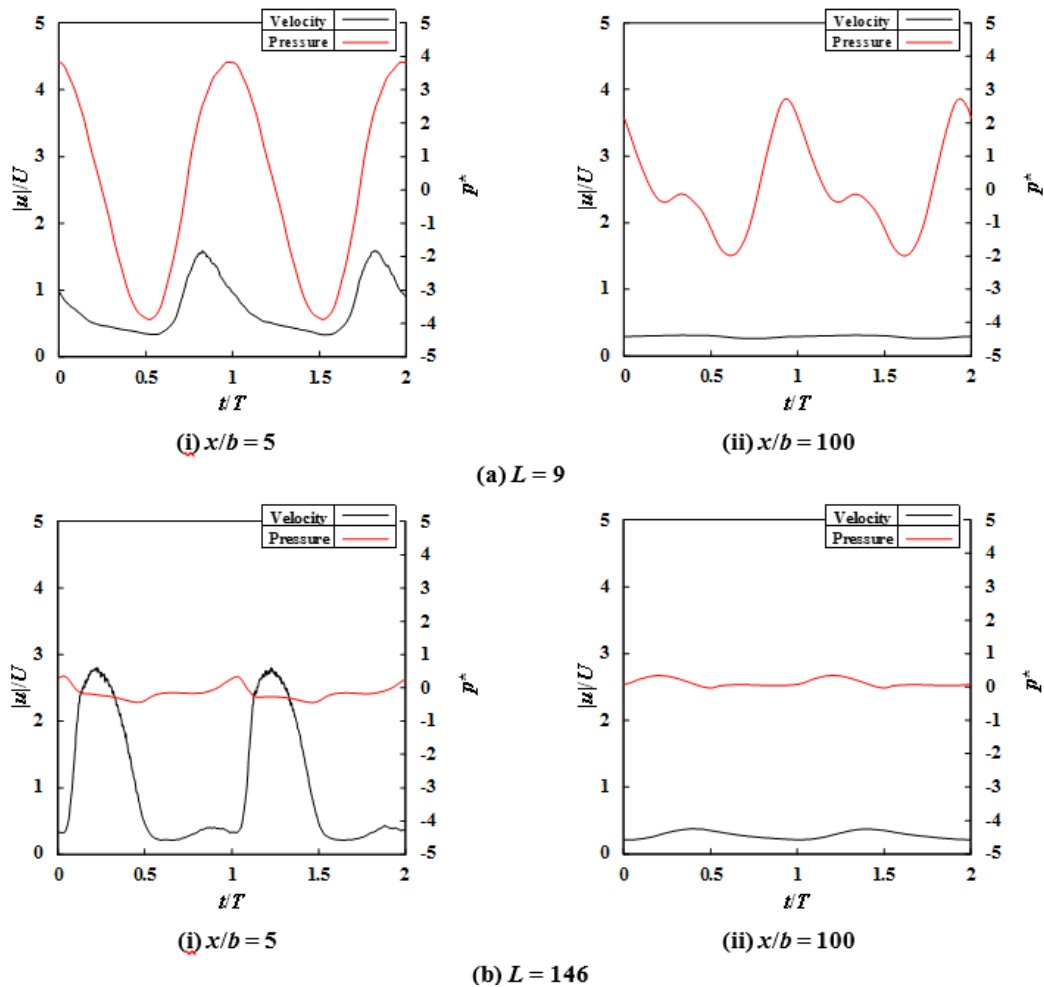


Fig. 8. Instantaneous velocity and pressure waveform along duct center from the experiment ($\Phi \approx 2.5, y/b = 0, z/b = 0$).

experiment and numerical simulation, respectively, for $\Phi \approx 2.5$ from the slot exit to the duct exit. The horizontal axis shows x/b and the vertical axis shows the dimensionless static pressure $p^* = p/0.5\rho U^2$. Both the experimental and the numerical results indicate that the wall pressure was restored from negative to positive pressure, reached a maximum pressure, and then decreased slightly owing to friction loss of the duct regardless of L . A study of the influence of L on the pressure restoration process indicated that the position at which pressure restoration started and reached the maximum shifted downstream with increasing L . This approximately corresponds to the position at which velocity distribution in the form of the jet flow changes to that of a duct-like flow from the observation of the time-averaged velocity distribution obtained from the numerical simulation. It is assumed to relate the case of free synthetic jet; it is known that the development point of a quasi-continuous jet flow (especially, increasing the expanding ratio of the jet-half width) shifts further

downstream with increasing L (Nishibe *et al.* (2011)). Therefore, in this study, it is considered one of the reasons for the dependency of L on the pressure restoration. Furthermore, the maximum pressure for $L = 9$ was smaller than that for $L = 82$ and 146 ; this trend corresponds to the performance and efficiency curves shown in Fig. 5.

Figure 7 shows the typical time-averaged velocity distribution on the mid-span ($z/b = 0$) from the numerical simulation for $\Phi \approx 2.5$. Panels (a)–(c) show the results for $x/b = 5, 50,$ and 100 , respectively. The horizontal axis shows y/b and the vertical axis shows the dimensionless time-averaged velocity based on the representative velocity \bar{u}/U . The dimensionless velocity profile at $x/b = 5$ was similar to that for a jet flow in a mixing region, and it gradually developed to a duct flow profile upon shifting downstream for $x/b = 50$ and 100 regardless of L . In addition, immediately downstream of the slot exit for $x/b = 5$, as shown in panel (a), the maximum

\bar{u}/U was confirmed to increase with L and the momentum calculated by integrating the square of the velocity distribution for $L = 82$ and 146 was larger than that for $L = 9$. Meanwhile, those for $x/b = 100$ were more similar than those at $x/b = 5$. Thus, without taking into account the unsteady

characteristics term and the energy loss with heat, the momentum differences between $x/b = 5$ and 100 in case of synthetic jets for $L = 82$ and 146 would be larger than those for $L = 9$. Therefore, we assumed

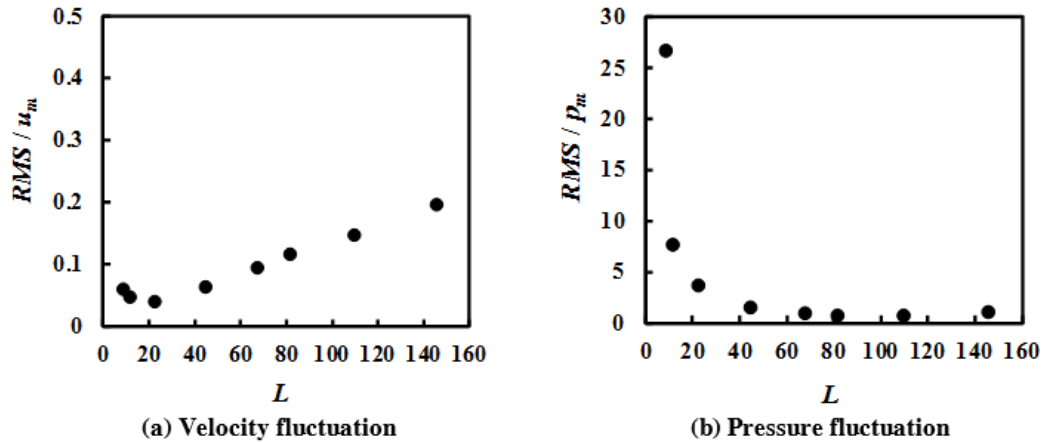


Fig. 9. Velocity and pressure fluctuations at duct exit-center from experiment. ($\Phi \approx 2.5, x/b = 100, y/b = 0, z/b = 0$).

that the momentum difference among the synthetic jets for $L = 9, 82$ and 146 is a possible reason for the difference in wall pressure under highly similar flowrates.

3.2 Unsteady Flow Characteristics

Figure 8 show the instantaneous velocity and pressure waveform along the duct center just downstream of the slot exit for $x/b = 5$ and the duct exit for $x/b = 100$ from the experiment. Panels (a) and (b) show the results for $L = 9$ and 146 , respectively. The black and red lines indicate the dimensionless velocity and pressure waveform, respectively. The qualitative trend of the influence of L on the velocity fluctuation was the same as that shown in Fig. 4. The amplitude of the velocity fluctuations for $L = 146$ was larger than that for $L = 9$ at all x/b values, and the velocity fluctuations for both $L = 9$ and 146 attenuate upon traveling downstream in the duct. The pressure fluctuations attenuated upon traveling downstream regardless of L , in the same way as the velocity fluctuations. In contrast, the amplitude of the pressure fluctuations for $L = 9$ was larger than that for $L = 146$ at all x/b values. Furthermore, the phase of the velocity and pressure fluctuations was not consistent for all L values. It should be noted that the pressure waveform at the duct exit has not only a dominant frequency corresponding to the actuator frequency but also multiples of the dominant frequency for $L = 9$; however, the influence of the fluctuation with multiple frequencies on the amplitude was considered to be limited.

To investigate the relation between L and velocity/pressure fluctuations in detail, the variation of the nondimensionalized RMS for these fluctuations based on the time-averaged velocity and pressure for $x/b = 100, u_m$ and p_m , for various L values are shown in Figs. 9(a) and 9(b), respectively. These results indicate that the RMS of the velocity fluctuations increased with L . This was attributed to

the collapse position of the vortex pairs generated near the slot exit shifting further downstream with increasing L , as shown by the velocity vectors and vorticity distribution for $L = 9$ and 82 in the maximum blowing through the numerical simulation (Fig. 3). This is supported by experiments that show that the dominant frequency component of the velocity waveforms in the duct center remains further downstream with increasing L and by the instantaneous vorticity distribution obtained from numerical simulation. In addition, Koso and Morishita (2014) experimentally showed that the tendency was the same as the position of the collapse vortex ring shifts further downstream for a free axisymmetric synthetic jet.

Meanwhile, the RMS for the amplitude of the pressure fluctuations increased with decreasing L . In addition, it was confirmed that these RMS values were approximately proportional to the frequency of the synthetic jet. This result was consistent that obtained from the one-dimensional Euler's equation of motion for oscillating flow streaming through a pipe to constant pressure.

From the velocity/pressure fluctuations described above, volume fluctuations at the slot exit generated by the synthetic jet induced flowrate fluctuations not only in the upstream of the slot but also in the downstream, even when the inertia of the duct downstream of the slot was relatively larger than that of the duct upstream (downstream:upstream ratio was approximately 22:1). Furthermore, the flowrate fluctuations downstream of the slot increased with L . The influence of the inertia balance of the synthetic jet fan on the performance/efficiency curves and unsteady characteristics should be the subject of future research.

These results showed that the appropriate operating condition of the proposed synthetic jet fan should be changed depending on the application. For example,

the synthetic jet fan for transporting fluids requires fans and pumps with high flowrate/pressure difference and continuous, stable, long-term operation. Within the range of the present study, the fluid machinery operating at $L = 45$ is recommended because this condition showed better performance in terms of both velocity and pressure fluctuations, which are relatively smaller than those at other values of L . On the other hand, when using jet ejectors/mixers, $L = 146$ is recommended because higher velocity fluctuations help to enhance the mixing of fluids with low pressure fluctuations.

4. CONCLUSION

The present study aimed to demonstrate the influence of the dimensionless stroke on the performance and unsteady characteristics of the synthetic jet fan through both the experiment and the numerical simulation. The performance and efficiency curves of the proposed synthetic jet fan were downward-sloping and concave down curves regardless of L , respectively. These tendencies were similar to those of a jet pump and fan that uses a continuous jet as the motive fluid and to those of previously reported synthetic jet fans. In addition, the maximum pressure coefficient Ψ_{max} and maximum flowrate coefficient Φ_{max} clearly increased with L for $9 \leq L \leq 45$ but showed no obvious differences for $45 \leq L \leq 146$. The differences in pressure performance and efficiency were assumed to occur because the velocity distribution for $x/b = 5$ for $L = 9$ was different from that for $L = 82$ and 146 . In addition, the pressure restoration position from the slot exit shifts downstream with increasing L ; this is related to the formative point of the synthetic jets.

A study of the unsteady characteristics of the synthetic jet fan showed that the RMS of the velocity fluctuations increased with L . Meanwhile, that of the pressure fluctuations decreased with increasing L . Therefore, within the scope of the present study, the suggested level of L for the operation of the fluid machinery as a fluid transport device is moderate (e.g. $L = 45$) to ensure stability and safety. Furthermore, as a mixing device, the fluid machinery should be operated with higher L (e.g. $L = 146$) for enhanced mixing.

ACKNOWLEDGEMENTS

The authors would like to thank Mr. Kazuki Ushikubo, Mr. Ryoichi Moriyama, Mr. Kyohei Kubo, and Mr. Daiki Haga of Tokyo City University for their help in conducting the experiments and data processing. This study was conducted with the support of a Grant-in-Aid for Scientific Research (15K05807), the Functional Micro-structured Surfaces Research Center of Kogakuin University (MEXT) and JGC Scholarship Foundation.

REFERENCES

Abdou, S. (2014). *Synthetic jet micropump*. Ph. D. thesis, McMaster University.
 Amitay, M., R. D., Smith, V., Kibens, E. D. Parekh,

and A. Glezer, (2001). Aerodynamic flow control over an unconventional airfoil using synthetic jet actuators. *AIAA Journal* 39(3), 361–370.
 Cattafesta, L. N. and M. Sheplak, (2011). Actuators for active flow control. *Annual Review of Fluid Mechanics* 43, 247–272.
 Holman, R., Y., Utturkar, R., Mittal, L. B. Smith, and L. Cattafesta, (2005). Formation criterion for synthetic jet. *AIAA Journal* 43(10), 2110–2116.
 Hoshi, M., I. Yoshikawa, and K. Sakai, (1964). Study of prototype 2-stage jet type pump. *Bulletin of JSME* 7(28), 737–745.
 Huang, B. J., J. M., Chang, C. P. Wang, and V. A. Petrenko, (1999). A 1-D analysis of ejector performance. *International Journal of Refrigeration* 22, 354–364.
 Ishizawa, T., K., Sato, K. Nishibe, and K. Yokota, (2015). Performance characteristics of a fan using synthetic jets. *Springer Proceedings in Physics* 185,109–115.
 Kobayashi, R., K., Nishibe, Y., Watabe, K. Sato, and K. Yokota, (2017). Vector control of synthetic jets using an asymmetric slot. *ASME J. Fluids. Eng.*, (in press).
 Koso, T. and M. Morita, (2014). Effects of stroke and Reynolds number on characteristics of circular synthetic jets. *Journal of Fluid Science and Technology* 9(2) 1–15.
 Koso, T. and R. Nakashima, (2008). Piezoelectric fan using a synthetic jet principle. *JSME* (in Japanese) 088(1), 1–2.
 Little, A. B., Y. Bartosiewicz, and S. Garimella, (2015). Visualization and validation of ejector flow field with computational and first-principles analysis. *Journal of Fluids Engineering* 137(5)1–12.
 Luo, Z.-B. and Z.-X. Xia, (2005). A novel valve-less synthetic-jet-based micro-pump. *Sensors and Actuators A: Physical* 122(1),131–140.
 Mahalingam, R., N. Rumigny, and A. Glezer, (2004). Thermal management using synthetic jet ejectors. *IEEE Transactions on Components and Packaging Technologies* 27(3),439–444.
 Narabayashi, T., Y., Yamazaki, H. Kobayashi, and Shakouchi, T. (2006). Flow analysis for single and multi-nozzle jet pump. *JSME International Journal Series B Fluids and Thermal Engineering* 49(4) 933–940.
 Narui, H. and S. Inagaki, (1991). Efficiency analysis of jet pumps without diffusers. *Transactions of the Japan Society of Mechanical Engineers. B* (in Japanese) 57(534), 575–580.
 Nishibe, K., Y., Fujita, K. Sato, and K. Yokota, (2011). Experimental and numerical study on the flow characteristics of synthetic jets. *Journal of Fluid Science and Technology*

6(4) 425–436.

- Ohuchi, H., T., Wadasako, T. Hosaka, and T. Osada, (2005). Fundamental study on a PZT jet pump. *Proceedings of the 6th JFPS International Symposium on Fluid Power*, 57–62.
- Park, J. H., S. Yokota and K. Yoshida, (2002). A piezoelectric micropump using resonance drive with high power density. *JSME International Journal Series C Mechanical Systems, Machine Elements and Manufacturing*, 45(2), 502–509.
- Sanger, N. L. (1970). An experimental investigation of several low-area-ratio water jet pumps. *Journal of Basic Engineering, Trans. of the ASME* 92(1),11–20.
- Shuster, J. M. and D. R. Smith, (2007). An experimental study of the formation and scaling of a round synthetic jet. *Physics of Tang Fluids* 34(1), 1–21.
- Tang, H. and S. Zhong, (2005). 2D numerical study of circular synthetic jets in quiescent flows. *Aeronaut. J.*109 (1092), 89–97.
- Whitehead, J. and I. Gursul, (2006). Interaction of synthetic jet propulsion with airfoil aerodynamics at low Reynolds numbers. *AIAA Journal*, 44(8),1753–1766.
- Xiao, L., X. Long, and J. Zhang, (2016). Shear cavitation in an annular jet pump under recirculation conditions. *Journal of Fluids Engineering*, 138(6),1–14.
- Xia, Q. and S. Zhong, (2012). A PLIF and PIV study of liquid mixing enhanced by a lateral synthetic jet pair. *Int. J. Heat Fluid Flow* 37, 64–73.
- Xia, Q. and S. Zhong, (2013). Liquid mixing enhanced by pulse width modulation in a Y-shaped jet configuration. *Fluid Dynamics Research* 45(2).
- Yamazaki, Y., A., Yamazaki, T., Narabayashi, J. Suzuki, and T. Shakouchi, (2007). Studies on mixing process and performance improvement of jet pumps. *Journal of Fluid Science and Technology* 2(1), 238–247.
- Yen, J. and N. A. Ahmed, (2012). Parametric study of dynamic stall flow field with synthetic jet actuation. *Journal of Fluids Engineering* 134(7), 1–8.
- Zhang, P., J., Wang, Y. Liu, and Y. Liu, (2007). Novel signal wave pattern for efficient synthetic jet generation. *AIAA J.* 45 (5) 1058–1065.